RESTORE

Renewable Energy based seasonal Storage Technology in Order to Raise Economic and environmental sustainability of DHC

Deliverable 3.1 –

Description of the numerical model for HP/ORC systems optimization and application to different test cases

Project Number: 101036766

Project Acronym: RESTORE

Project Title: Renewable Energy based seasonal Storage Technology in Order to Raise Environmental sustainability of DHC

Period covered by the report: from 01/10/2021 to 30/09/2023

Periodic report: NO

This project has received funding from the European Union's Horizon 2020 research and innovation programme under grant agreement No 101036766.

PROJECT INFORMATION SHEET	
Project Acronym	RESTORE
Project Full Title	Renewable Energy based seasonal Storage Technology in Order to Raise Environmental sustainability of DHC
Grant Agreement	101036766
Call Identifier	H2020-LC-GD-2020-1
Topic	Innovative land-based and offshore renewable energy technologies and their integration into the energy system
Project Duration	48 months (October 2021 – September 2025)
Project Website	www.restore-dhc.eu
Disclaimer	The sole responsibility for the content of this document lies with the authors. It does not necessarily reflect the opinion of the funding authorities. The funding authorities are not responsible for any use that may be made of the information contained herein.

INFORMATION SHEET	
Main Author(s)	Marco Astolfi (POLIMI) Dario Alfani (POLIMI)
Contributor(s)	Andrea Giostri (POLIMI) Giovanni Lozza (POLIMI) Nino Ravidà (POLIMI) Gianluca Valenti (POLIMI)

QUALITY CONTROL ASSESSMENT SHEET			
ISSUE	DATE	COMMENT	AUTHOR
V0.1	20/09/2023	First internal draft	Marco Astolfi (POLIMI) Dario Alfani (POLIMI)
V0.2	29/09/2023	Internal review completed	Other participants from POLIMI
V0.3	05/10/2023	Comments implemented	Marco Astolfi (POLIMI) Dario Alfani (POLIMI)
V0.4	10/10/2023	Review	Francisco Cabello (CENER)
V1.0	12/10/2023	Submission to the EC	Francisco Cabello (CENER)

Summary

The present deliverable presents the features, the operating principle and some results that can be obtained (among those already presented in international conferences and already passed through a two-step review process). According to task description the Numerical model can perform the constrained optimization of the system investigating non-conventional plant configurations and selecting the most appropriate working fluid(s). A numerical model has been implemented in Python 3.7 and integrated with REFPROP 10 in order to ensure a high accuracy of working fluid thermodynamic properties calculation. The numerical model is able to maximize system performance also providing a preliminary sizing of main components and techno-economic assessment based on RTE/A_{tot} that has been identified as the most appropriate figure of merit for preliminary screening of fluids and cycle optimal parameters also accounting for the heat exchangers sizing. The numerical model is flexible and able to include different types of RES and technologies or WEH for providing heat (at high and medium temperature) and electricity. In addition to what was reported in the Grant Agreement the code is also able to investigate reversible, coupled and decoupled cycles and perform Pareto front analysis. Code structure and main features are all implemented, and the code will be further improved till the end of the project as part of the activities related to further Tasks of WP3 (which will provide information on real size component performance in cooperation with Enerbasque in T3.2 and Turboden in T3.3 plus the quantification of off design in T3.4 and system dynamic in T3.5). Further tuning of the model to implement new schemes and scenarios will be implemented during Tasks of WP5 based on the specifications of the different use cases considered in *T5.4 Implementation, optimization, management & validation of RESTORE Use-Cases using the Simulation Web Platform* and its subtasks once they are available according to the Gantt implementation.

Table of Contents

1. Bibliographic review background

1.1. Pumped Thermal Energy Storage

Pumped Thermal Energy Storage (PTES) is an energy storage technology that uses electrical power during the charging phase to store heat at a temperature different from the ambient one and later exploits that heat to improve the performance of the discharging phase. From its general definition, PTES systems conceptually encompass most of the energy storage solutions different from electrochemical energy storage, flywheels and pumped hydro plants. For example, it is possible to conceptually classify as PTES commercial systems like the Adiabatic Compressed Air Energy Storage (ACAES) from Hydrostor [1] and the CO_2 battery from EnergyDome [2], where the compression heat is stored up to 400-600°C, and the Liquid Air Energy Storage (LAES) from Highview Power [3], that stores heat at both temperatures higher than the ambient one (from compressors intercoolers) and at cryogenic temperatures. These technologies are classified as semi-closed systems since the result of the charging phase is not only the storage of heat but also the storage of the working fluid as compressed air (CAES), liquid and gaseous CO_2 (CO_2 battery) or liquid air (LAES). Carnot battery technologies, on the contrary, are based on the adoption of closed thermodynamic cycles in both charging phase (heat pump for heat temperature upgrade) and discharging phase (heat exploitation with a power cycle) and thus they require only the storage of heat, potentially simplifying the system design and operation, and reducing the size for seasonal storage. Carnot batteries are differentiated by the selection of the thermodynamic cycle adopted for charging and discharging phase and the type of thermal energy storage adopted:

Thermodynamic cycle: the use of different thermodynamic cycles is proposed in literature and on the market: (i) closed gas Brayton cycles are commercialized by Malta Inc. [4] and also studied by SWRI [5], (ii) Steam Rankine cycles have been proposed by H2020 CHESTER project [6], (iii) Organic Rankine Cycles (ORC) are investigated by CHESTER [7] and RESTORE H2020 projects [8] while transcritical CO_2 cycles are proposed by Man Energy Solution [9] and Echogen [10]. Additionally, some systems architectures do not adopt a heat pump for the charging cycle preferring to directly dissipate electrical power to the HTF medium, usually air, and eventually to rocks as proposed by Siemens Gamesa [11], Pintail power [12] and Enel Green Power in cooperation with Brenmiller Energy [13].

Thermal storage: thermal storage can be classified as (i) sensible heat storage, in case liquid or gas streams are heated during the charging phase and then stored directly or by releasing heat to a high heat capacity medium, like in dual media thermocline solutions (rocks, metal spheres), (ii) latent heat storage, in case the heat is used in charging phase for melting a solid or vaporizing a liquid storage medium called Phase Change Material (PCM) (ice for low temperature storage, salts and their eutectic mixtures for temperatures up to 700-800°C [14]) and (iii) thermochemical storage, where the heat is used to support a specific reversible chemical reaction. Latent and thermochemical energy storage systems are mainly proposed for thermodynamic cycles with a pure working fluid phase transition (i.e., evaporation and condensation of organic fluids or CO_2), while sensible heat is preferable for Brayton cycles, supercritical CO_2 or non-eutectic fluid mixtures, thanks to better matching of the temperature profiles.

1.2. Carnot Batteries based on organic fluids

Previous studies have already shown the potential of ORC-based PTES systems considering both decoupled and coupled cycles architectures and, in this latter case, scientific literature has mostly focused on small-size systems that allow for the adoption of volumetric machines working as compressors in charge operation and expanders during discharge. Steger et al. [15] carried out a numerical multi-objective (electrical storage capacity and power-to-power efficiency) Pareto optimization to provide insights on the design and working fluid selection of a reversible HP/ORC system coupled to a latent energy storage. In particular, the authors highlighted the relevance of the working fluid enthalpy of vaporization in the process design, as it directly affects the mass flow rate and thus significantly influencing the investment costs of the system. Studying a similar system and considering the same working fluids (cyclopentane, R1233zd(E), Novec649 and R365mfc), Eppinger et al. [16] achieved power-to-power efficiencies above 60% for a heat source of 110°C, adopting both a sensible and latent heat storage for a pure electric system. The authors performed several parametric analyses and highlighted that, for most of the investigated cases, R1233zd(E) appeared to be the best choice thanks to the trade-off between system efficiency and environmental sustainability and safety. On the other hand, when considering also latent storage solutions, cyclopentane achieved the highest power-to-power efficiency. Limiting their analysis to reversible systems coupled to a sensible heat storage, Dumont et al. [17] developed a set of performance maps considering different combinations of working fluid, waste heat temperatures (50-90°C), storage temperature glide (5-15°C), and ambient temperature (0-40°C). The authors identified R1233zd(e), R1234yf, R11, R236ea and R245fa as the working fluids presenting the best performances. In the framework of the H2020 CHESTER project, Jockenhöfer et al. [18] investigated a decoupled system adopting butene for both the charging and discharging cycles. The results of the analysis showed that the investigated system can provide a net power ratio of 1.25 if a heat source temperature of 100°C and a heat sink temperature of 15°C are available. A similar system has been studied by Frate et al. [19] investigating 17 working fluid candidates but limiting the analysis to a sensible heat storage. The numerical results showed the possibility to boost the round-trip efficiency (RTE) to values higher than 1 thanks to the combination with a low-grade heat source. Considering a heat source temperature of 110°C, R1233zd(E) has been identified as the optimal fluid as it allows to achieve a theoretical maximum RTE of 1.3. However, is it important to note that the RTE is a figure that only considers the energy in form of electricity (i.e. electricity discharged vs electricity charged), non-considering the thermal energy required by the system in charge mode or the heat delivered in the discharge.

2. Numerical Model Description

The numerical code is implemented in Phyton 3.10 integrating REFPROP 10 [20] for the calculation of the working fluid thermodynamic and transport properties. **Figure 2.1-bottom** depicts the thermodynamic cycles in charge and discharge mode in a temperature-specific entropy (T-s) diagram for cyclopentane using the same thermodynamic streams indexing of **Figure 2.1-top**.

In this section a detailed description of the numerical code is provided, highlighting which are the implemented configurations that can be simulated (section **§2.1**) and the assumption and methodology to calculate the charging and discharging cycles (section **§2.2** and **§2.3**, respectively). Eventually, in section **§2.4.1** a description of the main outputs of the code together with their calculation routine is provided, while in section **§2.4.2** an explanation of the optimization routines implemented in the code is given.

2.1. Investigated cycle configurations

The numerical code is able to investigate three different system architectures:

- **Decoupled cycles**: two different cycles are designed for the charging (heat pump – HP) and the discharging cycle (power cycle – PC), respectively. As result, these systems involve a higher capital cost but also the following advantages: (i) two different working fluids can be selected for the two plants allowing to reach better thermodynamic performance and (ii) the heat exchangers can be designed for a single operating condition exploiting the most affordable HX architecture for each process (i.e., kettle reboiler for the HP evaporator and shell and tube condenser for PC with the organic fluid on shell side and cooling water in tubes).
- **Coupled cycles**: the same heat exchangers are adopted in the charging HP mode and the discharging PC mode. In this case, a single working fluid must be selected taking into account the different requirements of the two cycles. Moreover, heat exchangers must be sufficiently flexible to be operated in both modes: this is generally not a relevant issue for the recuperator, while it poses some limits for the low-pressure heat exchanger that must be able to switch from evaporator (HP) to condenser (PC). For this component a once-through heat exchanger should be selected and properly modelled in the numerical code considering working fluid flowing in the tubes and water in the shell side.
- **Reversible cycles**: the same heat exchangers and the same machines are adopted in the charging HP mode and the discharging PC mode. Also in this case, a single working fluid must be selected considering the different requirements of the two cycles. As for the *Coupled cycles* case, heat exchangers must be sufficiently flexible to be operated in both modes and once-through heat exchanger should be selected and properly modelled in the numerical code considering working fluid flowing in the tubes and water in the shell side. Additionally, the same machine is used for the fluid compression (HP) and expansion (PC): volumetric machines are the most recommended option in this case as scroll (below 10kW) and screw (below 100kW) architectures being able to be operated in both modes. In case of *Reversible cycles*, the design shall be carried out in compression mode and the

performance as expander are then calculate with correction curves that will be provided by Enerbasque during activities of **T3.2**.

Figure 2.1-top represents the scheme of the proposed coupled cycle architecture in both charging (left) and discharging (right) mode since from preliminary considerations it looks the most adequate one in terms of efficiency/cost trade off and the only one appropriate for large scale systems (>1MW) connected to district heating networks. To exploit the matching between the isothermal reactor and iso-thermobaric phase transition in both HP condensation and PC evaporation, the working fluid phase change occurs directly within the reactor, which is thus designed as a coil heat exchanger inside the stirred reactor. This choice has been carried out in agreement with TUW according to the high heat transfer coefficients during fluid phase transition (evaporation/condensation) and the need to maximize performance that would be otherwise penalized by heat transfer fluid temperature variation, especially in case of low temperature rise heat pump cycles.

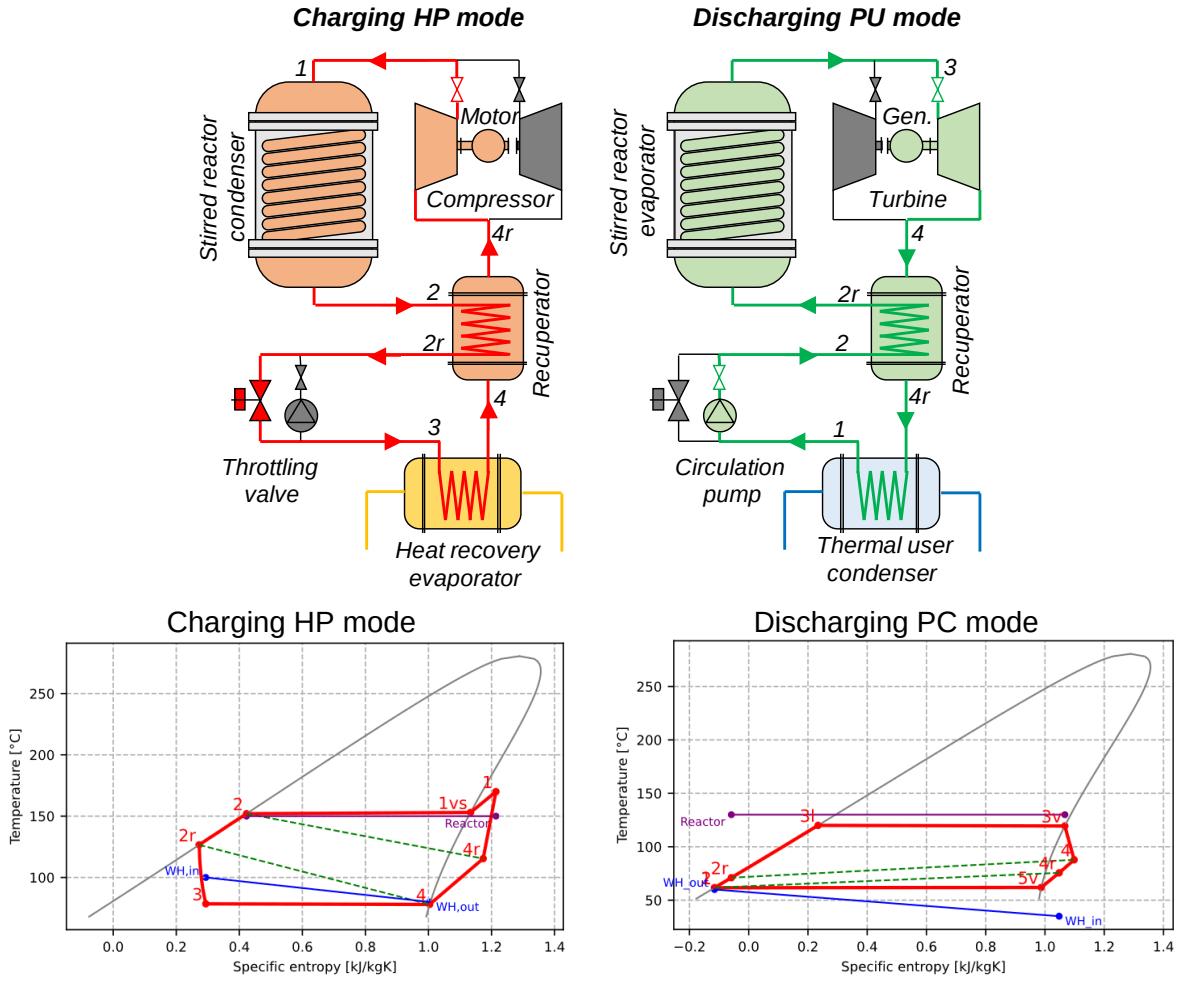

***Figure 2.1** – (top) Coupled Cycles Configuration Scheme Adopting Reversible Heat Exchangers, (bottom) T-s Diagrams For (left) Charging and (right) Discharging Cycles Using Cyclopentane In Coupled Cycle Configuration.*

Additional phase separation vessels can be included in order to control throttling valve and turbine admission thermodynamic conditions: they are not reported in the figure and are currently not modelled in the numerical code since they do not affect the energy and mass

balances of the system and in overall, the performance. The scheme of a *Decoupled system* is conceptually very similar, with the only differences related to the duplication of the heat exchangers, the need of two reactors (or a double coiled one), the compressor and turbine installed on different loops, and the avoidance of three-way valves for the working fluid flow inversion. Finally, the *Reversible cycle* case is as the *Coupled cycle* case but for the use of the same machine for compression and expansion rather than two different components.

While the numerical simulation of decoupled cycles is quite straightforward and it has already been proposed in literature (see section **§1.2**), while the assessment of the performance of *Coupled cycles* and *Reversible cycles* is less investigated and is generally based on simplified assumptions on the operating parameters of the discharging PC mode, such as the pressure drops and the pinch point temperature differences in the heat exchangers. However, to properly evaluate the impact on discharge cycle performance of the PC pressure levels and mass flow rate, which are necessarily different from the charging cycle ones, it is necessary to develop specific numerical tools to account for the heat exchangers operation in off-design mode (plus the volumetric machine performance for the *Reversible cycles*)

As explained in detail in section **§2.2.1,** in POLIMI numerical code it has been decided to size the system heat exchangers for the coupled cycle in charging mode and to compute the PC performances and operating conditions by maintaining the same geometrical parameters of the heat exchangers (number and length of the tubes, heat transfer surface, etc.). This choice is motivated by preliminary calculations that shown how, for the same assumptions (pinch point temperature differences, pressure drops, tube diameters and fins density) the overall area is higher for the HP rather than for the PC mode and because the performance of the HP has a greater impact on the system Round Trip Efficiency with respect to the PC efficiency.

2.2. Heat pump simulation (charging mode)

2.2.1. Heat pump thermodynamic calculation

The solving scheme of the charging mode is reported in **Figure 2.2** on the left, showing the interconnections between assumptions and thermodynamic streams calculation.

The main inputs code required are:

- the heat source inlet and outlet temperatures, which should be set according to the considered application (industrial low temperature waste heat, geothermal energy or mid temperature solar energy).
- the reactor charging temperature, which should be set according to the experimental results carried out by the Technical University of Wien (TUW) on the selected salt hydration, the dehydration processes and its operational parameters such as concentration of solids in oil or the reactor operating pressure.

The heat pump cycle calculation routine starts by computing the evaporation and condensation temperatures (points 2 and 4, see **Figure 2.1**) from the outlet temperature of the heat source ($T_{HS,out}$) and the operating temperature of the chemical reactor in charging mode ($T_{react,CH}$), assuming the heat exchangers pinch point temperature differences ($\Delta T_{pp,COND}$ and $\Delta T_{pp,EVA}$).

Saturated vapor condition (point 1v) is calculated by assuming a fixed pressure drop in phase transition defined as a temperature difference between inlet and outlet condition in order to make a fair comparison between fluids having different critical points and so very different saturation pressures at the same temperature level. Additionally, as a further option in the numerical code, it is possible also to define the total pressure drop in the condenser component both as a relative or as an absolute pressure drop. The compressor outlet temperature (point 1), i.e. the maximum cycle temperature, is set by the user and could be the object of optimizations or sensitivity analysis to understand its impact on system performance. Its maximum value has been set to 180°C, which is nowadays a reasonable limit for the temperature reached by high temperature heat pumps and also because increasing the compressor outlet temperature for the same reactor charging temperature implies a strong increase of de-superheating area and required surface area in the stirred reactor.

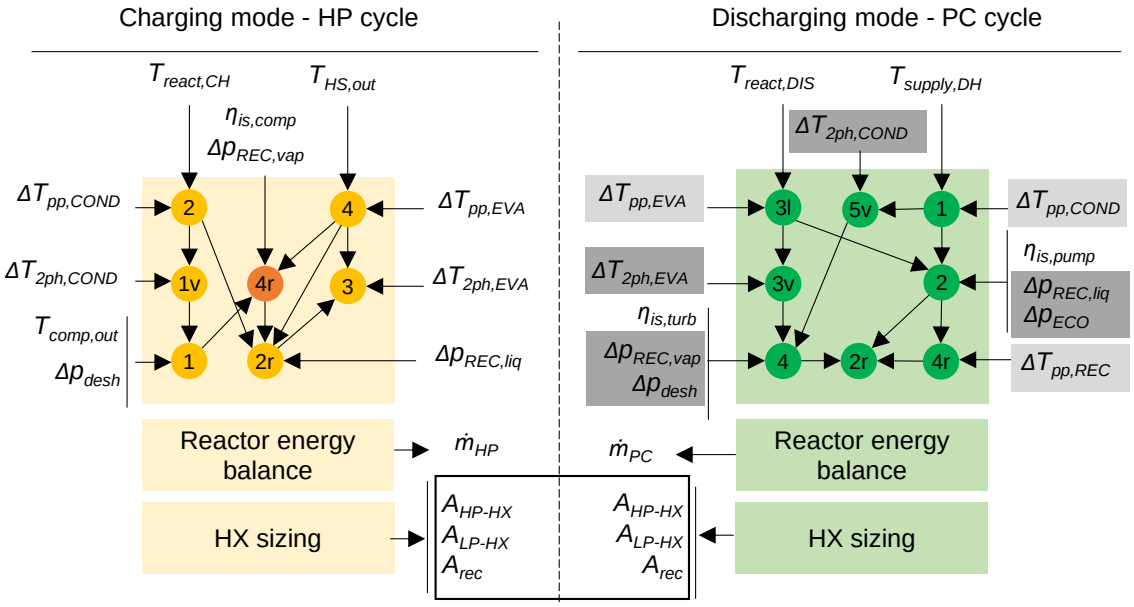

Figure 2.2: *solving scheme for the HP (left) and PC cycle (right). For the hp cycle, point 4r requires an iterative calculation. Only for the coupled cycle architecture, parameters in light grey boxes are obtained by matching heat exchangers surfaces, while pressure drops in dark grey boxes are calculated.*

The compressor inlet temperature (point 4r) is then determined from the knowledge of compressor outlet temperature (point 1), the compressor pressure ratio and the assumed compressor isentropic efficiency ($\eta_{is,comp}$): as the compressor inlet temperature (4r) generally results higher than the saturation temperature at evaporation pressure (1v), the use of a recuperator is required for preheating vapours by cooling down the saturated liquid (2) before the throttling valve inlet (2r). The duty and size of the recuperator are dependent on the fluid complexity and the desired compressor outlet temperature: for very complex fluids with strongly overhanging saturation dome the recuperator is always required to avoid two-phase flow compression, for mid-complexity fluids it is required only above a certain compressor outlet temperature, while in case of simple molecule fluids (i.e., ammonia) the recuperator is not required. Throttling valve outlet condition (3) is eventually determined by assuming an isenthalpic process from the recuperator hot side outlet condition (3r). Pressure drops for both

sides of the recuperator ($\Delta p_{REC,vap}$ and $\Delta p_{REC,liq}$) are an input of the numerical code and can be set as absolute or relative values. **Table 2.1** reports all the numerical code inputs required for the calculation of HP cycle. Eventually, the working fluid mass flow rate is calculated from an energy balance at the reactor being the thermal duty $\dot{Q}_{reactor,CH}$ set by the user and the heat pump coefficient of performance (COP_{HP}) is computed through **equation 1** after having calculated the compressor consumption with **equation 2**.

$$COP_{HP} = \frac{\dot{Q}_{reactor,CH}}{\dot{W}_{comp,el,HP}} \quad (1)$$

$$\dot{W}_{comp,el,HP} = \dot{m}_{HP} \cdot \frac{(h_1 - h_{4r})}{\eta_{mot} \cdot \eta_{mec,comp}} \quad (2)$$

***Table 2.1**: required inputs for the computation of the HP thermodynamic cycle.*

Numerical code required input for HP calculation	
Heat source and storage constraints	**Example values**
Reactor thermal power input, kW	1000
Charging reaction temperature $T_{react,CH}$, °C	150
Heat source inlet temperature $T_{HS,in}$, °C	100
Heat source outlet temperature $T_{HS,out}$, °C	80
HP cycle components parameters	**Suggested value**
Evaporator equivalent pressure drop $\Delta T_{2ph,EVA}$, °C	0.5
Condenser equivalent pressure drop $\Delta T_{2ph,COND}$, °C	1
De-superheater relative pressure drop	0.5%
Recuperator relative pressure drop (hot/cold)	2%
Compressor isentropic efficiency $\eta_{is,comp}$	80%
Compressor mechanical efficiency, $\eta_{mec,comp}$	97%
Motor electrical efficiency, η_{mot}	97%
Evaporator pinch point temperature difference, °C	2
Condenser pinch point temperature difference, °C	2

2.2.2. Heat pump heat exchangers sizing

Once all the HP thermodynamic streams are determined as reported in section **§2.2.1**, the sizing of the heat exchangers is carried out by adopting a discretized (the default value set by the code is 50 sections, but it can be changed by the user) and iterative approach which depends on the type of heat exchanger and the architecture of the system (coupled cycles/decoupled cycles). The effect in the heat transfer process of possible fouling is neglected for the design of all the heat exchangers while all the other inputs required by the numerical code related to heat exchanger sizing are reported in **Table 2.2**, along with the default value set by the numerical code.

- **High pressure heat exchanger (HPHX):** fluid condensation and de-superheating are carried out in the coiled tubes of the stirred reactor acting as a once-through heat exchanger. Tube diameter and tube thickness are set by the user, and inlet fluid velocity is determined in order to match the assumed overall pressure drop. The number of tubes is then calculated, and the tube length and overall heat transfer area are eventually retrieved knowing the local overall heat transfer coefficient obtained by the combination of internal

heat transfer coefficient (working fluid side) and the external one (stirred reactor side), plus the metal conductive resistance. Gnielinski correlation [21] is adopted for vapor working fluid de-superheating, Cavallini correlation [22] is implemented for condensation (requiring an additional internal iterative procedure for the determination of the tube wall temperature), while the external heat transfer coefficient is assumed constant and set by the user (a default value equal to 2000 W/m^{2}K, as suggested from [23]). Pressure drops are calculated only considering the frictional contribution for vapor and two-phase flow regime.

- **Low pressure heat exchanger (LPHX):** in the case of coupled cycles architecture the fluid evaporation is carried out in a shell-and-tube once-through heat exchanger and, also in this case, the number of tubes is found iteratively to match the assumed pressure drops. Liu and Winterton correlation [24] is adopted for the heat transfer coefficient in flow boiling conditions (requiring an additional internal iterative procedure for the determination of the heat flux) while the external heat transfer coefficient is calculated with Zukauskas correlation [25] for both liquid and gaseous streams by assuming a fixed longitudinal and transversal tube pitch, a fixed tube arrangement and a fixed baffle spacing with respect to shell diameter. Working fluid pressure drops in evaporation are calculated only considering the frictional contribution. The arrangement of the heat exchanger can be modified from co-current to counter-current by the user to investigate different heat exchanger sizing. In the case of decoupled cycles, a conventional kettle reboiler is adopted. In this case, pressure drops are set to zero and the calculation is non-iterative. Cooper correlation [26] is adopted for evaporation side while, for hot water, Gnielinski correlation is adopted with the same tube diameter and a water velocity equal to 2 m/s to avoid damage, wear and tear of the HX pipes.
- **Recuperator**: a finned tube battery heat exchanger is implemented considering liquid fluid flowing in tubes and vapor flowing on the external finned surface in cross flow. The number of tubes and tube pitch calculation relies on an iterative procedure to match the pressure drops on liquid and vapor sides, respectively. Gnielinski and Zukauskas correlations are used for the computation of liquid and vapor heat transfer coefficients, respectively. A fixed Aext,tot/Aint ratio can be set and a default value equal to 11 is adopted if the user does not insert one.

***Table 2.2**: required inputs for the preliminary sizing of the heat exchangers and their default value.*

Numerical code required input for heat exchangers sizing	**Default value**
Heat exchangers tubes	
Tube internal diameter, mm	25
Tube thickness, mm	2
Tube internal roughness, mm	10-3
Material	SS316
HP evaporator (low pressure HX)	
Tube arrangement	Staggered
Ratio of longitudinal tube pitch to ext. diameter	1.25
Ratio of transverse tube pitch to ext. diameter	1.25
Relative baffle spacing to shell diameter	0.2
Recuperator	
Ratio of longitudinal tube pitch to ext. diameter	1.75
Ratio of transverse tube pitch to ext. diameter	1.75
Finned external to internal surface ratio	11

2.3. Power cycle simulation (discharging mode)

A saturated organic Rankine cycle is considered for the power cycle (PC). As heat is released at a constant temperature from the thermochemical reactor, the adoption of fluid superheating is not advantageous in this specific case as it would simply result in a reduction of evaporation pressure and a penalization of cycle performance according to the adoption of an isothermal thermochemical reactor. Furthermore, by adopting complex working fluids it is possible to avoid two-phase flow expansion even starting from saturated vapor conditions (points 3v to 4 in **Figure 2.1**). In the case of decoupled cycles, it is possible to adopt or not an internal recuperator, while for coupled configurations the component is present if already required by the heat pump cycle and there is no-need to bypass it since it allows to increase discharge mode mass flow rate and power output.

The numerical code main inputs consist of the reactor discharging temperature and the district heating supply and return temperatures. In the case of *Decoupled cycles* architecture, the calculation procedure is very similar to the charging one (section **§2.2.1**) and it is reported in **Figure 2.2** on the right. In this case the numerical code requires the specification of the pinch points temperature differences, and the pressure drops in the evaporator, condenser and recuperator. Sizing of heat exchangers follows the same procedure already explained for the charging cycle (see section 3.2.1) with the only difference related to the condenser: in this case, a shell and tube architecture is implemented with district heating water flowing in the tubes and vapor condensing on the shell side. Nusselt modelling [27] is adopted for film condensing while for cold water the Gnielinski correlation is adopted considering a water velocity of 2 m/s as default value.

Differently, in case of *Coupled cycle* architectures, the determination of evaporation temperature, condensation temperature, recuperator pinch point temperature difference and pressure drops in each heat exchanger is based on the off-design operation of the components already sized in charging mode. Knowing the number of tubes, their length and the heat transfer area, the fluids outlet thermodynamic conditions are determined iteratively adopting the same correlations for heat transfer and pressure drops already implemented in charging mode. Even for the PC the low-pressure heat exchanger (condenser) is operated in co-current flow arrangement in order to have the largest local temperature difference in the de-superheating process, which is characterized by the lowest working fluid heat transfer coefficient. This approach allows to significantly increase the system RTE as discussed in section **§3.1.2**. In the case of coupled cycles, the reactor power $\dot{Q}_{reactor,DIS}$ in discharging mode is set equal to the reactor power in charging mode, thus considering the same charging and discharging time. Of course, this assumption is not mandatory, and the numerical code user has the possibility to modify this option to achieve a final design of the system tailored to the specific investigated application that may differ in the average charging and discharging power. For example, it is reasonable that residential applications would require a larger heat pump size, working fewer hours a year during summer and exploiting the availability of electrical renewables only in off-peak periods, and a smaller size power unit working steadily during winter period for a longer time. In this latter case, power cycle performance would benefit since all the heat exchangers would be oversized in discharge mode (off design operation will be analysed in **T3.4**). Additionally, a thermal integration can be considered in discharging mode if a heat source (renewable or waste heat) is available also during winter period. In this case, a

secondary heat exchanger is considered in series after the PC condenser, allowing to reduce the PC condensing temperature and improving the system discharge performance.

Table 2.3 reports all the numerical code inputs required for the calculation of PC cycle. Finally, the power cycle working fluid mass flow rate is calculated from an energy balance at the reactor and the power cycle efficiency coefficient of performance (η_{PC}) is computed through **equation 3** after having calculated the turbine and pump consumptions with **equation 4** and **equation 5**, respectively.

$$\eta_{PC} = \frac{\dot{W}_{turb,el,PC} - \dot{W}_{pump,el,PC}}{\dot{Q}_{reactor,DIS}} \quad (3)$$

$$\dot{W}_{turb,el,PC} = \dot{m}_{PC} \cdot (h_{3v} - h_4) \cdot \eta_{gen} \cdot \eta_{mec,turb} \quad (4)$$

$$\dot{W}_{pump,el,PC} = \dot{m}_{PC} \cdot \frac{(h_1 - h_2)}{\eta_{mot} \cdot \eta_{mec,pump}} \quad (5)$$

***Table 2.3**: required inputs for the computation of the PC thermodynamic cycle.*

Numerical code required input for PC calculation			
Storage and district heating constraints	**Example value**		
Reactor thermal power output, kW	1000		
Discharging reaction temperature $T_{react,DIS}$, °C	130		
DH water delivery temperature $T_{DH,del}$, °C	60		
DH water return temperature $T_{DH,ret}$, °C	35		
	Decoupled	***Coupled***	**Reversible**
PC cycle components parameters	**Suggested values**		
Expander isentropic efficiency η_{turb}	90%	90%	*Calc.*
Pump hydraulic efficiency η_{pump}	80%	80%	80%
Expander mechanical efficiency $\eta_{mec,turb}$	97%	97%	97%
Pump mechanical efficiency $\eta_{mec,pump}$	97%	97%	97%
Motor electrical efficiency η_{mot}	97%	97%	97%
Generator electrical efficiency η_{gen}	97%	97%	97%
Evaporator pinch point temperature difference, °C	2	*Calc.*	*Calc.*
Condenser pinch point temperature difference, °C	2	*Calc.*	*Calc.*
Recuperator pinch point temperature difference, °C	3	*Calc.*	*Calc.*
Evaporator equivalent pressure drop $\Delta T_{2ph,EVA}$, °C	1	*Calc.*	*Calc.*
Condenser equivalent pressure drop $\Delta T_{2ph,COND}$, °C	0.5	*Calc.*	*Calc.*
Economizer relative pressure drop	2%	*Calc.*	*Calc.*
De-superheater relative pressure drop	0.5%	*Calc.*	*Calc.*
Recuperator relative pressure drop (hot/cold)	2%	*Calc.*	*Calc.*

2.4. Figures of merit and optimization

2.4.1. Main figures of merit calculation

The H2020 RESTORE project has the main goal to provide an effective solution for unlocking the possibility of dispatching a large amount of thermal energy on seasonal terms. This result could be obtained independently on the working fluid selected, the compressor outlet temperature or the cycle architecture adopted. On the contrary, dispatchability and storage of electricity is a secondary feature whose performance actually varies consistently depending on the system design. For this reason, the overall electrical RTE of the system should be selected as one the main figure of merit for the comparison of different working fluids and cycle configurations. Electrical RTE is defined as the ratio between the net electrical energy released by the power cycle and the electrical energy absorbed by the heat pump cycle, as reported in **equation 6**, where h_{DIS} and h_{CH} are the number of discharging and charging hours, respectively.

In this preliminary analysis, the additional auxiliaries consumption related to the water circulation and stirring of the reactor is neglected for both the charging and discharging cycle.

$$RTE = \frac{(\dot{W}_{turb,el,PU} - \dot{W}_{pump,el,PU}) \cdot h_{DIS}}{\dot{W}_{comp,el,HP} \cdot h_{CH}} \quad (6)$$

It must be noted that if the assumption of the same charging and discharging hours holds and the storage system has an efficiency of 100%, the definition of **equation 6** is equivalent to the product between the heat pump coefficient of performance COP_{HP} and the power cycle electrical efficiency η_{PC}.

When considering the tradeoff between system performance and investment cost for these kinds of systems, as the power-to-heat ratio of this application is rather low (high heat pump COP and rather low power cycle efficiency), the system capital cost is likely dominated by heat exchangers equipment. For this reason, in addition to system electrical RTE, the ratio between RTE and overall heat exchanger surface (RTE/A_{tot}) is computed as it represents an important parameter from a techno-economic perspective.

Finally, the volume ratio and maximum volumetric flow rate for both compressor and turbine are computed by the numerical code as they represent important quantities for the comparison of turbomachinery size and cost for different working fluids. Maximum volumetric flow rates (compressor intake and turbine discharge) directly affect turbomachinery frontal area while the number of stages is generally determined by the need of overall volume ratio repartition, since blade loading is generally limited for high molecular mass working fluids, as in this case.

It must be also noted that, since the performance of the different components (in particular the turbine and the compressor) is not affected by the equipment size, RTE, RTE/A_{tot} and turbomachinery volume ratio (Vr) are only a function of the working fluid, while mass and volumetric flow rates can be scaled up and scaled down linearly for different system size.

2.4.2. Optimization routine description

According to the tool description provided above, the code execution is straightforward being all the relevant parameters already fixed and the only free variable is the choice of the working fluids to be adopted in charging and discharging mode that is handled as a sensitivity analysis. The only exception is the case of *Decoupled cycles* thermally integrated in discharging where the condensation temperature shall be optimized to maximize PC efficiency. In the case of *Coupled cycles* and *Reversible cycles,* the main numerical issue that requires a proper and robust numerical routine is the verification of the off design (and the volumetric expander) behaviour in discharging that requires handling a large number of variables (see **Table 2.4**) and difference functions to be set to zero and related to heat transfer equipment area and expander efficiency. In this case, both a solver or an optimization algorithm (minimizing the sum of the quadratic errors on the difference objectives) and both options are implemented. Also in this case, for thermally integrated cycles in discharge the condensing temperature can be further optimized. Results related to this approach are reported in section **§3.1.**

Differently from the previous approach, an alternative method for the identification of the most promising cycle and fluid combinations is to expand the analysis by relaxing some of the inputs and considering them as optimization variables rather than assumed values. If the lower and upper bounds of each optimization variable are set in order to explore a vast region of possible solutions, it could be necessary to implement routines for inspecting the obtained results and to adopt penalization functions which allow to discard non-feasible solutions. In addition, an initial guess of the optimization variables must be specified to properly initialize the optimization algorithm close enough to the solution, consequently reducing the computational time and increasing the accuracy of the final solution. To properly investigate the design and operating parameters of the RESTORE system several optimization algorithms available in the Pymoo (Multi-objective Optimization in Python) module [28] are implemented in the numerical code to minimize or maximize the objective functions specified by the user (round-trip efficiency, heat exchangers surface, RTE/A_{tot},) while satisfying specified design constraints. The choice of the most suitable optimization algorithm is strongly dependent on the number of optimization variables, the number of objective functions and the kind of application considered.

Considering the systems under study and from a general point of view, by adopting larger heat transfer surfaces it is possible to increase the system overall RTE thanks to the lower irreversibilities in the heat transfer processes, at the expenses of a higher heat exchanger investment cost that likely represent the main share of capital cost according to the high heat/electrical power ratio of the adopted thermodynamic cycles (high COP for the HP and low PC thermal efficiency). The trade-off between RTE and total heat transfer area is investigated with a Non-dominated Sorting Genetic Algorithm (NSGA) for multi-objective optimization to define the Pareto front and identify the most promising techno-economic solutions. The optimization variables considered for this analysis are six design parameters that characterize the heat exchanger dimensions as reported in **Table 2.4** while some results that can be obtained with this method are reported in **§3.2.** The main impact from techno-economic perspective of the selected parameter is:

- The pinch point temperature differences (ΔTpp) in the high-pressure (condenser in charge mode) and low-pressure (evaporator in charge mode) heat exchangers, which directly affect the heat transfer average temperature difference and thus the heat

exchangers UA parameter. Once the storage temperature is assumed and the ΔTpp defined, the minimum and maximum pressure of the charging cycle are also determined. The higher the ΔTpp, the lower is the heat transfer area with a consequent penalization in performance because of the increased pressure difference in the HP cycle and the lower pressure ratio in the PC one. The pinch point temperature difference in the recuperator is not considered as optimization variable as it results from the specification of the compressor outlet temperature, which fixes the thermal duty of the recuperator. In a precedent study it has already been highlighted the dependency of the overall system RTE and heat transfer surfaces from the compressor outlet temperature, so in this work the outlet temperature from the compressor has been fixed at 180°C considering the limit of existing high temperature heat pumps.

- The pressure drops (Δp) on the working fluid side, for all the heat exchangers of the system, affects the working fluid velocity in the tubes. The higher the specific pressure drop is, the higher the heat transfer coefficient and lower the area of the heat exchanger for the same duty and average ΔT but also lower the system performance due to the additional compression ratio in charging and reduction of the expansion one in discharging.

***Table 2.4**: Heat pump cycle heat exchangers design parameters range for Pareto front analysis.*

Parameter	**Example range**
HP Evaporator pinch point temperature difference, °C	[0.5 - 10]
HP Condenser + desuperheating pinch point temperature difference, °C	[0.5 - 10]
HP Evaporator overall pressure drops working fluid side, %	[1% - 20%]
HP Condenser + desh overall pressure drops working fluid side, %	[1% - 20%]
HP recuperator pressure drops working fluid low pressure side, %	[1% - 20%]
HP recuperator pressure drops working fluid high pressure side, %	[1% - 20%]

3. Examples of analysis attainable with the developed code

In this section are proposed two examples of possible analysis that can be carried out with the developed numerical code. A first analysis is presented in Section **§3.1**, with the purpose of comparing the techno-economic performances of systems based on coupled and decoupled cycles. The second part **§3.2** is related to some examples of Pareto front analysis.

3.1. Working fluids screening and comparison

Results are obtained by investigating the performance of the *Coupled cycle* system with 16 different working fluids (preselected from a wider pool of over 30 fluids) while the performance of the *Decoupled cycle* system is obtained by combining the results for the heat pump and power cycle obtained for all the working fluids, for a total amount of 256 cases. **Table 3.1** lists the selected working fluids and their critical temperature, Global Warming Potential (GWP) and Health, Fire and Instability hazard (HFI) indexes as defined by National Fire Protection Agency (NFPA). Most of the preselected fluids are hydrocarbons, a promising class of fluids for this application, spanning in a large range of critical temperatures and having low GWP (generally below 5 likely also for fluids where the index is not reported due to the lack of available data) although they are flammable and, in some cases, slightly toxic (Benzene, Xylenes, Dimethyl carbonate). Only a few halogenated fluids with sufficiently high critical temperature for this specific application have been included while several others (i.e., perfluoro-propane, R227ea, perfluoro-cycle-propane, perfluoro butane) have been excluded since they show extremely high GWP (between 3000 and 10000), and their use is discouraged by their progressive phase out. Siloxanes are not included in the list as well due to their high critical temperatures, which makes them not the preferable choice for such low temperature applications.

Table 3.1: *Investigated Working Fluids and Their Critical Temperature, Global Warming Potential (GWP) And HFI Indexes as Defined By NFPA.*

#	Fluid	T_{crit}, °C	GWP	NFPA		
				H	F	I
1	Trans-2-butene	155.46	N.A.	1	4	0
2	Cis-2-butene	162.60	N.A.	1	4	0
3	Novec649	168.66	1	3	1	0
4	R365mfc	186.85	794	0	4	1
5	Isopentane	187.20	5	1	4	0
6	Isohexane	224.55	<1	2	3	0
7	Cyclopentane	238.57	5	1	3	0
8	Cyclohexane	280.45	2	1	3	0
9	Dimethyl carbonate	283.85	<1	3	3	0
10	Benzene	288.87	N.A.	2	3	0
11	Octane	295.59	4-6	1	3	0
12	Para-xylene	343.02	N.A.	2	3	0
13	Meta-xylene	343.74	N.A.	2	3	0
14	Decane	344.55	4-6	1	2	0
15	Orto-xylene	357.11	N.A.	2	3	0
16	Propyl-cyclohexane	357.65	4-6	1	3	0

Two preliminary discussions on the effect of compressor outlet temperature and heat exchangers arrangement are provided only for cyclopentane, as it has been identified as one of the most promising working fluids for this specific case study.

3.1.1. Effect of compressor outlet temperature

Increasing the compressor outlet temperature has a positive effect on the system performance. For a given fluid, with a fixed minimum temperature of the renewable (or waste heat) source and a fixed reactor charging temperature, a higher compressor outlet temperature implies a higher compressor inlet temperature: compressor specific work increases but the fluid mass flow rate reduces because of the larger working fluid enthalpy change between reactor inlet (1) and outlet (2). For a fixed reactor duty, the compressor power decreases leading to an increase of COP_{HP}. In the case of coupled systems, there is an additional benefit related to the increase of recuperator heat transfer surface required to preheat working fluid vapours before compression, as it also allows to increase η_{PC} in discharging mode. **Figure 3.1.a** depicts the sensitivity analysis on compressor outlet temperature for cyclopentane in a *Coupled cycles* architecture. It is possible to highlight that the RTE increases from 33.8% to 36.4% (+7.7%) when passing from 160°C to the maximum allowable compressor outlet temperature, equal to 180°C. This beneficial effect is mainly due to an increase of COP_{HP}, which passes from 3.3 to 3.5 (+5.6% on relative base), and only marginally from an improvement of η_{PC}, which increases from 10.1% to 10.3% (+2% on relative base). **Figure 3.1.b** depicts the trend of heat exchanger surfaces against compressor outlet temperature: as the compressor outlet temperature increases, recuperator size clearly increases because of the larger thermal duty and the lower pinch point temperature difference. However, for cyclopentane, the recuperator size is marginal with respect to the other heat exchangers. Low pressure heat exchanger surface just marginally increases due to slightly larger thermal duty of the component due to the higher COP_{HP}. Finally, the heat transfer area of the stirred reactor (high pressure heat exchanger), which represents the largest component of the system, shows an increasing trend with compressor outlet temperature as the larger temperature difference in the de superheating process does not compensates for the lower local heat transfer coefficient of this section.

As result, the total heat exchangers surface increases by 19% at maximum compressor outlet temperature, causing a reduction of the RTE/A_{tot} parameter, which accounts for the tradeoff between efficiency gains and increase in heat transfer equipment size. **Figure 3.1.c** reports the effect of compressor outlet temperature on turbomachinery parameters, namely volume ratio and volumetric flow rate. Compressor volume ratio (Vr) slightly decreases since the compression process is farther from the saturation dome and characterized by lower real gas effects while volumetric flow rate at compressor intake reduces since the reduction of mass flow rate is not balanced by the decrease of inlet fluid density caused by the temperature increase. Regarding the expander, the effect on volume ratio is nearly negligible since the compressor outlet temperature only slightly affects the evaporation temperature in discharging mode, while the turbine outlet volumetric flow rate increases because of the slightly lower condensing pressure.

In conclusion, the increase of compressor outlet temperature for cyclopentane benefits the system performances by 7.7%, but causes an increase of 19% of heat exchangers surfaces and a reduction of 6% of turbomachinery dimension and thus seems to be profitable only in cases with very high remuneration of electricity during the discharge operation. These

considerations in relative terms are generally valid for most of the investigated fluids but those characterized by very low critical temperatures. Another observation is related to the possibility to operate fully reversible cycles where also the compressor/expander is actually the same component operated reversibly: the volume ratio in expansion is slightly lower than in compression (around -10%), thus implying the feasibility of operating the same volumetric machine in both operative modes.

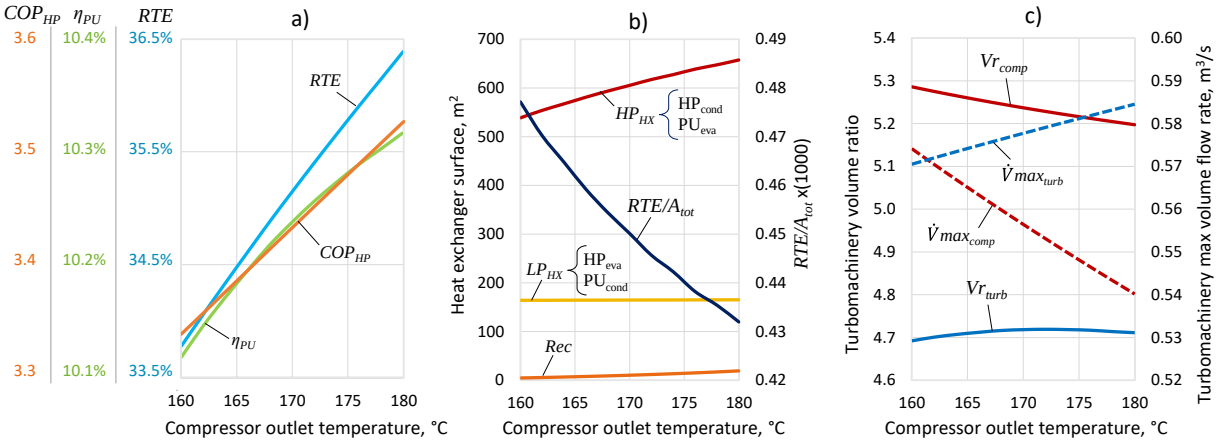

Figure 3.1: *trend of relevant parameters for coupled system with cyclopentane vs. Compressor outlet temperature: a) COP_{HP}, η_{PC} and system RTE, b) heat exchanger area and overall RTE/A_{tot}, c) volume ratio and volumetric flow rate for compressor and turbine.*

3.1.2. Effect of heat exchangers arrangement (co-current vs counter-current)

A sensitivity analysis is carried out by varying the flow arrangement of the low-pressure heat exchanger namely adopting the four combinations given by co-current and counter-current flow arrangement in charging mode (HP evaporator) and discharging mode (PC condenser).

Table 3.2 summarizes the results of this analysis applied to the coupled cycle architecture working with cyclopentane fluid. Having a counter-current arrangement in the HP charging cycle (design mode) implies a larger heat exchanger heat transfer area, even if this difference is rather limited (around 7%), and a slightly lower COPHP. On the contrary, flow arrangement in discharging PC mode has a much higher impact on system performance: a counter-current disposition implies a much higher condensation temperature for the power unit (around +3°C), a larger pinch point (around +5.5°C) as a consequence of a larger heat transfer surface required for the fluid de-superheating. On the contrary, adopting a co-current disposition the efficiency of the power unit is increased (+0.5 point of efficiency) thanks to a lower condensation temperature, as well as the overall RTE of the system (+2 point of efficiency and +6% on relative base).

***Table 3.2**: results of the sensitivity analysis on the low-pressure heat exchanger flow arrangement*

Case	A	B	C	D
HP_{eva} **PC_{cond}**	**Counter-c** **Counter-c**	**Co-c** **Counter-c**	**Counter-c** **Co-c**	**Co-c** **Co-c**
LP_{HX}, m^2	176.4	164.8	176.4	164.8
PC T_{cond}, °C	64.7	65.6	61.6	62.0
PC $\Delta T_{pp,cond}$, °C	6.4	7.4	1.6	2
COP_{HP}	3.41	3.43	3.41	3.43
η_{PC}	9.86%	9.71%	10.30%	10.24%
RTE	**33.6%**	**33.3%**	**35.1%**	**35.15%**

3.1.3. Working fluid selection for coupled cycle architecture

Figure 3.3 depicts the trend of RTE and RTE/A_{tot} as a function of the compressor outlet temperature for the 16 fluid candidates in a coupled system configuration. It is possible to highlight that by increasing the compressor outlet temperature the RTE (**Figure 3.2.a**) increases for all the investigated fluids and that most of them show a quite similar RTE: in particular, adopting low critical temperature fluids does not appear as a promising solution mainly due to the low achievable COPHP. On the contrary, the discussion related to the RTE/A_{tot} (**Figure 3.2.b**) parameter is less trivial since the trend of the total heat transfer area is different depending on the fluid critical temperature.

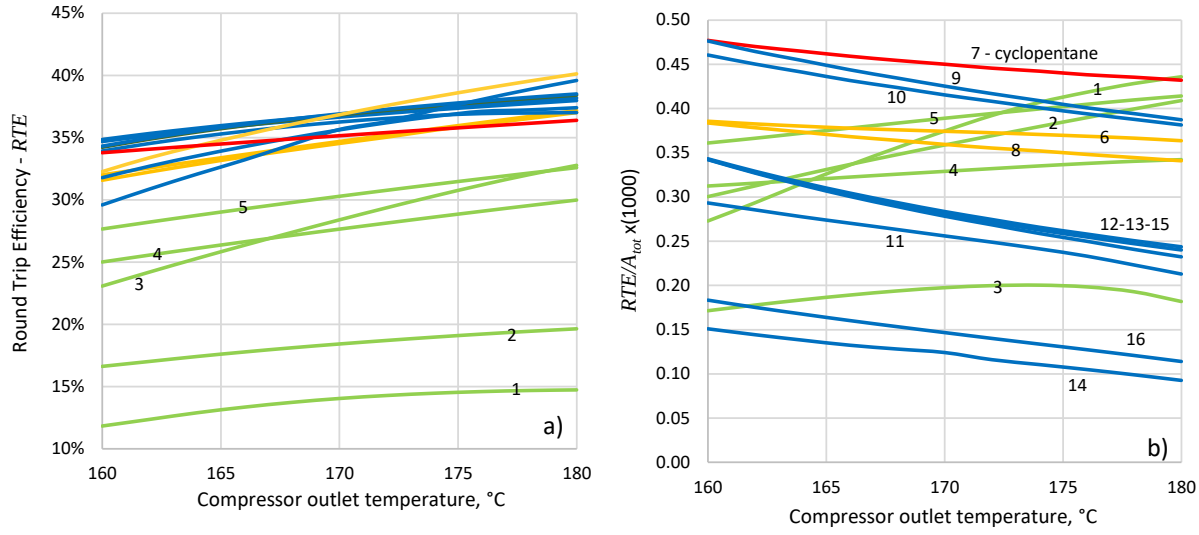

***Figure 3.2**: trend of relevant parameters for coupled system vs compressor outlet temperature: a) system RTE, b) overall RTE/A_{tot}.*

By increasing the compressor outlet temperature for low critical temperature fluids (green lines in figure) the de superheating section is characterized by relatively high local heat transfer coefficients (thanks to the higher fluid density) that, combined with the higher local temperature difference, actually entails a reduction of high-pressure heat exchangers surfaces (i.e., coiled heat exchanger in the stirred reactor) and thus an increase of the RTE/A_{tot} parameter. For fluids with intermediate critical temperatures (yellow lines in figure), as cyclopentane (red line), the increase of heat transfer area implies a slight reduction of the RTE/A_{tot} parameter. Finally, higher critical temperature fluids (blue lines) show very low condensing pressure in HP mode involving very low heat transfer coefficients for organic vapors and a soaring of the heat transfer area required for fluid de superheating, being this section always designed with a fixed pressure drop, and thus RTE/A_{tot} is further penalized. Cyclopentane (red line) stands out as a promising fluid from both RTE and RTE/A_{tot} perspectives in the whole range of compressor outlet temperatures. A deeper analysis is provided focusing on an intermediate compressor outlet temperature equal to 170°C and reporting the figures of merit as a function of fluid critical temperature. **Figure 3.3.a** depicts the trend of RTE, COPHP and ηPU: it is possible to highlight that, apart from the butene isomers, all the other fluids show nearly the same PC efficiency while they strongly differ in COP_{HP}, which increases by 70% within the fluid critical temperature range investigated in this work.

As result, RTE initially strongly benefits by adopting working fluids with a higher critical temperature and then flatten above a critical temperature of around 250°C. **Figure 3.3.b** depicts the total HXs area and COP_{HP} parameter against fluid critical temperature.

The total heat transfer area increases with the fluid critical temperature since this causes an exponential decrease of cycle pressures and thus, being the heat exchanger designed with the same relative pressure drops, a strong penalization in the heat transfer coefficients: in particular, the recuperator gradually become a relevant share of the overall heat transfer area. RTE/A_{tot} parameter accounts for these effects and shows a trend with a maximum. Finally, **Figure 3.3.c** depicts the trend of volume ratio and volumetric flow rates. The volume ratio is relatively constant and lower than 10 for fluids with critical temperature below 300°C while rapidly increases for higher values implying the use of a multi-stage turbine and compressors. Similarly, volume flow rates exponentially increase with fluid critical temperature, leading to larger and more expensive machines.

Those results lead to the conclusion that the choice of the working fluid shall also include techno-economic considerations since the adoption of a fluid with a too low critical temperature may penalize the system due to the lower RTE while the adoption of a fluid with an excessive critical temperature would involve an increase of heat exchanger (i.e., higher total heat transfer area) and turbomachinery cost (i.e., higher frontal area and the number of stages). Among the investigated fluids, cyclopentane looks particularly promising, being able to reach a high RTE (>35%), to maximize the RTE/A_{tot}, to limit the volume ratio to reasonable values for single stage (or, at maximum, two-stages) radial machines and it does not show excessive volume flow rates.

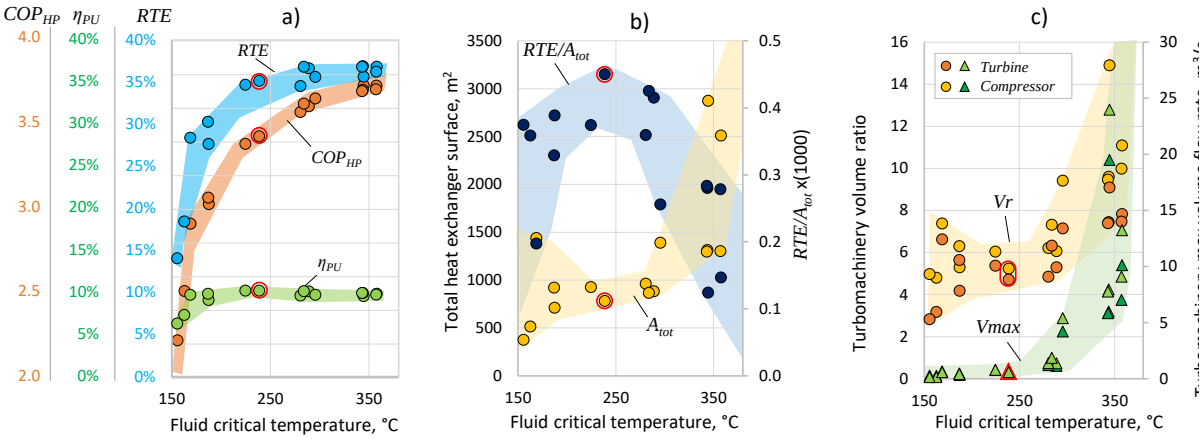

***Figure 3.3**: trend of relevant parameters for the coupled system with all fluids vs critical temperature: a) HP_{COP}, PC efficiency and system RTE, b) heat exchanger area and overall RTE/A_{tot}, c) volume ratio and volumetric flow rate for turbomachinery. The red envelopes on the markers identify cyclopentane.*

3.1.4. Working fluid selection for decoupled cycle architecture

The adoption of two different separate cycles for the charging and discharging operation may be of interest with the goal of maximizing system performance, thanks to the selection of the most suitable working fluids for the HP and the PC cycle, and the design of dedicated heat exchangers for both systems relying on more conventional component types. **Figure 3.4** reports colored maps of *RTE*, total heat transfer area and overall RTE/A_{tot} parameter obtained for the 256 working fluid combinations, considering a compressor outlet temperature of 170°C. RTE (**Figure 3.4.a**) increases remarkably by adopting high critical temperature fluids for the HP cycle while it is less affected by working fluid choice on the PC cycle, where the maximum performance achievable is rather stable against fluid choice, as already highlighted in **Figure 3.3.a.**

From a mere thermodynamic performance perspective (i.e., RTE maximization), there is no need to select two very different fluids for the HP and the PC cycles, thus leading to results similar to coupled cycles systems: optimal combination is Decane and Propyl-cyclohexane for HP and PC cycles respectively, reaching a RTE equal to 42.5%. On the contrary, from a techno-economic perspective it would be interesting to adopt a high critical temperature fluid for the HP cycle and to prefer a lower critical temperature fluid for the PC cycle in order to attain a smaller heat transfer area of the heat exchangers (**Figure 3.4.b**), a lower turbine size (lower volume ratio and volumetric flow rate) but still a competitive PC efficiency. As result, the decoupled cycles system with the minimum RTE/A_{tot} (**Figure 3.4.c**) adopts Dimethyl carbonate (DMC) for the HP cycle and Cis-2-butene for the PC cycle, but reaches an RTE/A_{tot} value equal to 0.303, which is more than 30% lower than the best coupled cycle architecture with cyclopentane discussed in section **§3.1.1**. Other fluid combinations, especially those adopting high critical temperature fluids for the PC, are strongly penalized and, from a techno-economic perspective, can only reach RTE/A_{tot} values one order of magnitude lower.

Those considerations demonstrate that the use of two decoupled cycles is not likely to be a promising solution for this specific case. However, the analysis also suggests that different

conclusions can be obtained in cases where the charging and discharging cycles are different in size and annual operating hours, namely a large size HP and a small size PC (or vice versa): in this case, the different working fluid mass flow rates and power input/output may lead to the adoption of different working fluids to obtain a more feasible turbomachinery and heat exchangers design.

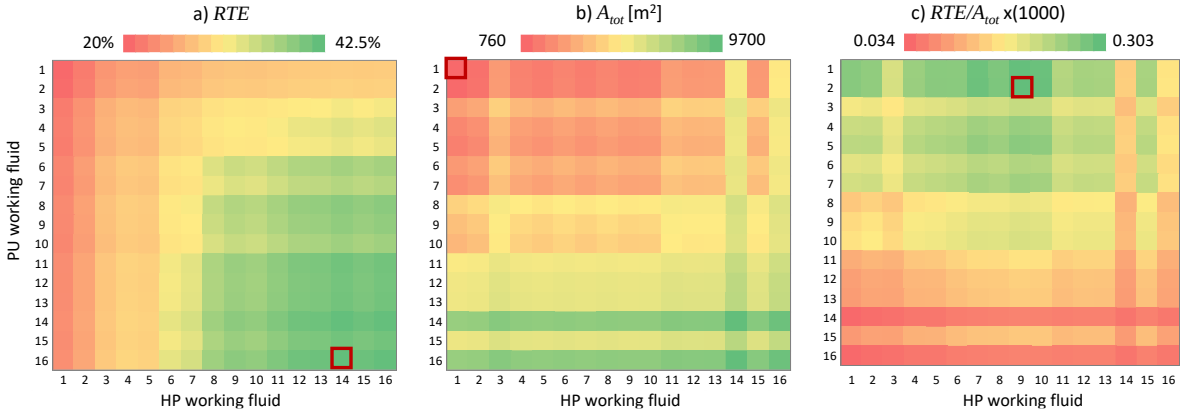

***Figure 3.4**: contour maps of the most relevant parameters for decoupled system for all the working fluids combinations: a) system RTE, b) heat exchanger area and, c) overall RTE/A_{tot}*

3.2. Selected working fluids pareto front analysis

These results refer to the comparison between cyclopentane and two other fluids candidates in both a RESORE like cogenerative case (CHP) where the heat of condensation from the ORC is used for the DH and a pure electric stand-alone case where the main goal is to dispatch renewable electricity (ELE CASE). This section is divided in two parts: the first one focuses on the analysis of the results obtained for cyclopentane with a description of the Pareto fronts and the trend of variables adopted in the analysis, the second part focuses on the comparison of cyclopentane with two other fluid candidates.

The results of the multi-objective optimization are reported in **Figure 3.5** for both the electricity-only (ELE) configuration (**Figure 3.5.a**) and the cogenerative (CHP) one (**Figure 3.5.b**), considering cyclopentane as the working fluid. The figure reports the tradeoff between electrical RTE (x-axis) and the total heat transfer surface of the system (y-axis): in blue it is depicted the overall population explored by the NSGA optimizer in the last generation, while in red it is possible to notice the optimal solutions on the Pareto front, i.e. the set of non-dominated solutions.

As expected, the electricity only system can achieve higher values of round-trip efficiency (up to around 70% which is a value comparable to current Li-ion batteries and PHES) thanks to the much lower condenser pressure in the power cycle (discharging mode), which allows for a higher enthalpy drop in the turbine and thus an improved net power output of the system.

From the graph of **Figure 3.5.a** and **Figure 3.5.b** it is possible to notice that the trend of the overall heat transfer surface versus the electrical RTE of the system is strongly not linear: above a certain RTE threshold, an increase of the system performance can be attained only with an exponential growth of heat transfer surfaces due to the non-linear correlation between heat transfer temperature differences and heat transfer surfaces. This RTE threshold is equal to around 0.5 for the ELE configuration and to around 0.4 for the CHP system, as it is possible

to notice from the evident soaring of heat exchangers surfaces above these values. It is also worth mentioning that the maximum RTE/A_{tot} (**Figure 3.5.c** and **Figure 3.5.d**) is not obtained by pushing the round-trip efficiency to the maximum achievable values and the optimal point is found for both cases in a region of the Pareto front characterized by rather low RTE values. In particular, the maximum RTE/A_{tot} is found between RTE values of 0.3 and 0.4 for the ELE configuration, while it is characterized by lower values (0.25-0.35) for the CHP system, as it could be expected due to the overall lower RTE values of such configuration. In addition, for the CHP system, the RTE/A maximum value is lower than in the ELE case (-30%).

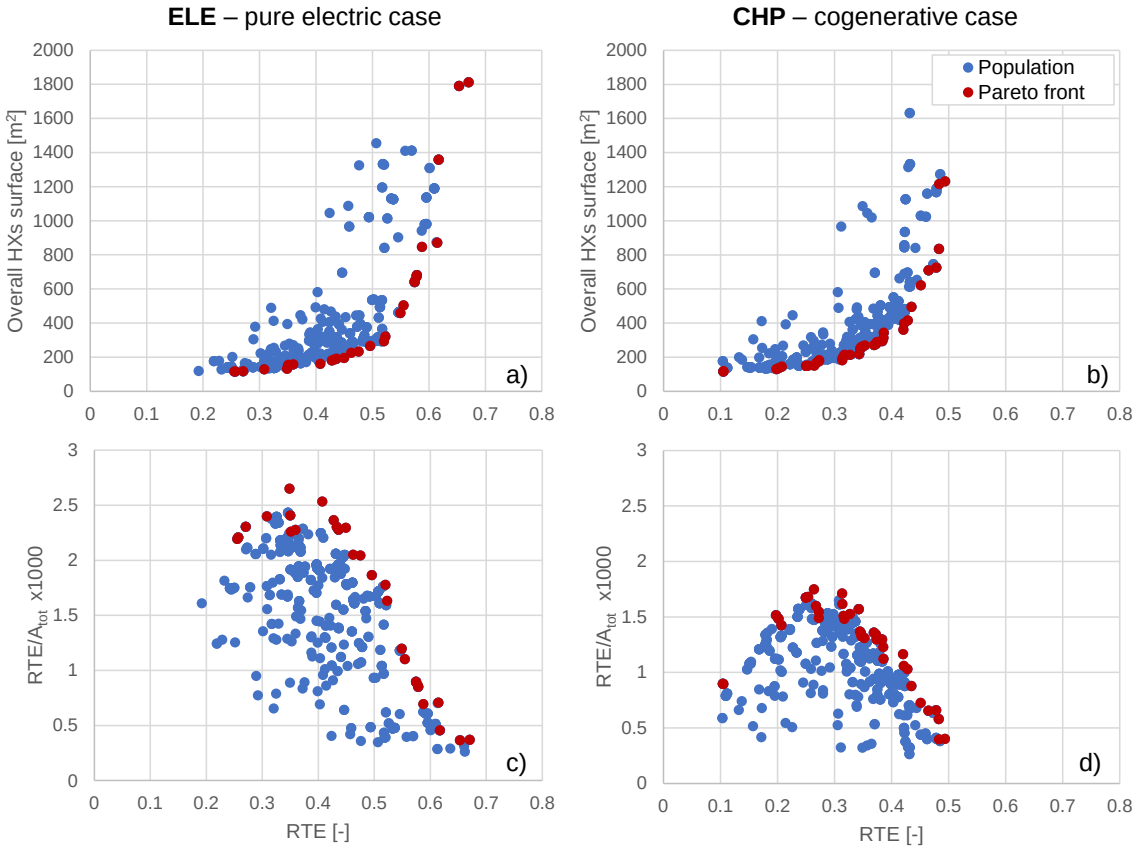

***Figure 3.5**: Pareto front of optimal solutions (red) for the electricity only (a) and cogenerative case(b). RTE/Atot ratio for the electricity only (c) and cogenerative (d) cases.*

The trends of the Pareto optimal values for the pinch point temperature differences of the low-pressure heat exchanger (evaporator in HP mode) and of the high-pressure heat exchanger (condenser in HP mode) are depicted in **Figure 3.6.a** and **Figure 3.6.b**, respectively. For both system configurations the trend of these optimization variables is similar: the optimization variable which is mainly responsible for the trade-off between RTE and overall HX surface is the ΔTpp,LP, as this parameter linearly varies between the minimum and maximum RTE of both systems, being pushed to the lower bound only for combinations of very high RTE and HXs total surface. Similar considerations can be made for ΔTpp,HP, even if it is possible to notice that the optimizer set its value really close to the upper bound in the low-RTE range of the Pareto front, denoting that it could be useful to slightly relax the upper bound on this variable.

These results also suggest that the assumption considered for the precedent analysis of using a pinch point temperature difference of 2°C to design the heat exchangers in the HP/charging cycle of the cogenerative system [8] could be improved by adopting values around 5°C and 7°C for the LP HX and HP HX respectively, in order to attain the maximum RTE/A_{tot} ratio.

As the pressure drops affect less significantly the trade-off between system performance and overall HX surface, their trend on the Pareto front is less linear and tends to be more scattered. However, as expected, it is possible to notice that the working fluid side relative pressure drop in the low-pressure HX tends to decrease for higher RTE values. This trend can be explained considering that this pressure drop has two opposing effects on the HX surface as (i) higher fluid velocities lead to higher convective heat transfer coefficients and (ii) higher pressure drops in two-phase conditions (in this case evaporation), lead to lower average heat transfer temperature differences considering a fixed ΔTpp,LP. However, as the first effect is more significant than the second, the higher the LP HX pressure drop, the lower this heat exchanger surface. On the other hand, even if this variable does not affect the COP of the heat pump, as it only increases or decreases the pressure drop foreseen by the lamination valve, it strongly influences the condensation temperature of the power cycle, significantly affecting the power output attainable in discharge mode.

In contrast, the pressure drop in the cold and low-pressure side of the recuperator (heat pump mode) reported in **Figure 3.6.c** and **Figure 3.6.d** also affects the COP of the charge cycle as, at fixed compressor outlet temperature and pressure, it increases the compressor pressure ratio and thus its electrical consumption. For this reason, to maximize the COP of the heat pump the optimizer tends to select the optimal values of this variable closer to the lower bound.

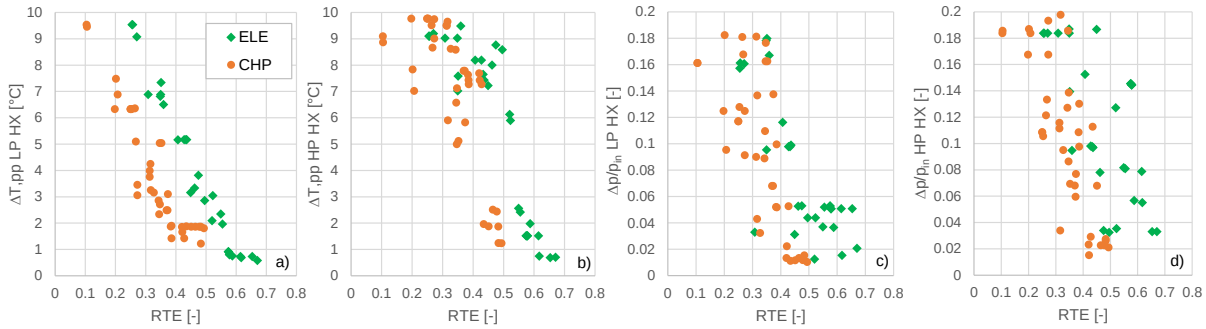

***Figure 3.6**: Trend of some of the optimization variables along the Pareto front for the electricity only (green) and cogenerative (orange) cases*.

Figure 3.7 depicts the comparison in both the ELE and CHP case of cyclopentane and the other two fluids, NOVEC649 (representative of fluids with a lower critical temperature) and octane (representative of fluids with a higher critical temperature). It is possible to highlight that octane can potentially reach RTE slightly higher than cyclopentane especially in the CHP case, but this is generally obtained with heat exchangers with an overall heat transfer area that, for the same RTE, can be up to 60% higher in the interval of RTE where the maximum of RTE/A_{tot} is located. This aspect results from the larger ratio between the latent heat of vaporization and the enthalpy variation in compression/expansion, which is a consequence of the distance between the thermodynamic cycle and the fluid critical point, which leads to lower operative pressures thus requiring higher heat transfer surfaces to achieve reasonable pressure drops

in the components. Only in some ELE cases at very high heat transfer area, octane can reach the same RTE with a lower heat transfer area. NOVEC649 analysis leads to almost opposite considerations: the proximity of the critical point implies a reduction of heat pump performance because of the lower latent heat of condensation at high temperatures, which is not compensated by the compact heat exchangers that can be designed with higher operating pressures. *RTE/A*$_{tot}$ parameter is penalized and generally reaches values up to half the corresponding value achievable with cyclopentane. Maximum reachable *RTE* are penalized as well and cannot go over 60% in ELE case and 50% in CHP one.

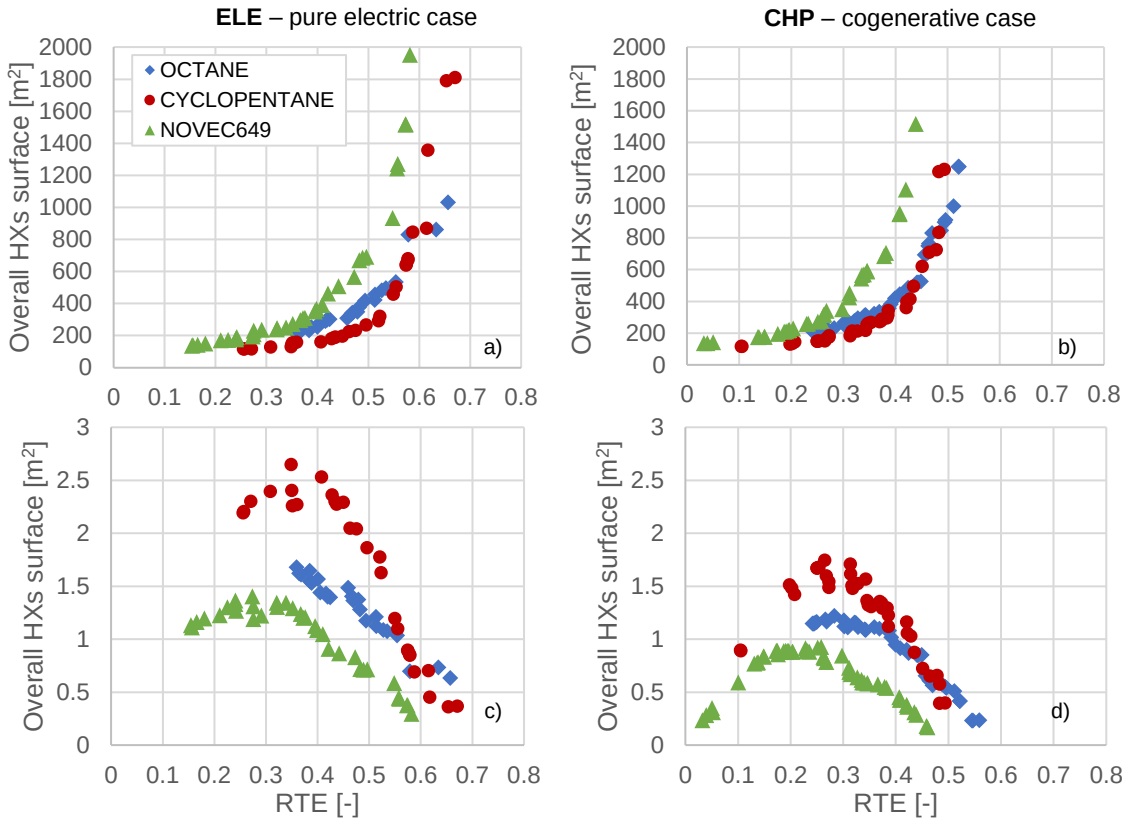

Figure 3.7: *Comparison of the Pareto front and RTE/A*$_{tot}$ *obtained with cyclopentane (red), NOVEC649 (green) and octane (blue) for both the electricity only (left) and CHP (right) cases.*

4. Conclusions

In this deliverable, the initial investigations have primarily concentrated on the RTE and RTE/A_{tot} as figure of merits. However, it is important to emphasize that the present model can also be employed for the analysis of heat consumption and delivery within organic cycles and future figures of merits involving these terms can be considered. The model that has been developed will prove to be of significant importance for forthcoming project endeavours, particularly in relation to "Task 3.2 - Design for upscaling the HP/ORC solution for small Districts" and "Task 3.3 - Design for upscaling the HP/ORC solution for large Districts." Furthermore, it will be further refined and enriched with the findings from these tasks.

Main outcomes are:

- From a purely thermodynamic perspective, mid-temperature PTES systems based on organic fluids are a promising solution thanks to the better matching between the isothermal thermochemical reactor and the working fluid phase transition, which allows to minimize the maximum temperature reduction when passing from charging to discharging mode.
- Maximum achievable RTEs in the range between 35% and 40% are comparable with those attainable with H_2 storage from electrolysis plus power production in gas turbines or fuel cells, making the proposed solution a possible asset in future energy markets requiring seasonal electricity storage. It is also worth noting that storing electricity is a positive side effect available from this technology implementation which main goal is to dispatch thermal energy thus RTE is an important parameter for screening promising fluids but for a real use case the analysis shall also include the impact on the revenues from selling of the thermal energy.
- The use of coupled cycles, although more complex from control perspective, allows to significantly reduce the capital cost of the system, still guaranteeing good thermodynamic performances (RTE>35%). In this case, cyclopentane appears to be one of the most recommended working fluids from a techno-economic point of view, as it reaches a high RTE (35%) and the maximum RTE/A_{tot} index (0.45). It also presents small volumetric flow rates and limited compressor and turbine volume ratios, simplifying the design of the turbomachinery. Use of hydrocarbons is interesting from an environmental point of view (GWP equal to 5 and null ozone depletion potential), while their flammability is an issue already faced in most of the ORC units installed worldwide. Alternatively, high critical temperature refrigerant fluids could be used but they are currently in phase-out due to their high GWP and their cost is getting prohibitive.
- Decoupled cycles can be of interest in case the use of a reversible system is not possible due to the difficulties in designing and operating heat exchangers alternatively as condensers with a de-superheating section and evaporators with an economizer. In this case, it would be possible to find a combination of fluids able to achieve RTE over 30% and reasonable RTE/A_{tot}.
- Considering Pareto front analysis, the round-trip efficiencies for the pure electric case are around 10% higher than cogenerative case for the same overall heat transfer area,

thanks to the lower condensation pressure and ranges between 20% for very low heat exchangers dimension, up to 70% but requiring an exponential increase of the heat transfer area. Maximum RTE/A_{tot} parameter, that for high heat to power ratio cycles as in this case can be considered a reasonable techno-economical figure of merit, is obtained at rather low RTE around 35% confirming the results obtained with a less general approach. The more relevant parameters for the analysis are the two-phase flow heat exchangers temperature differences while the pressure drops, due to the nonlinear relation with global heat transfer coefficient, have a lower impact on the overall heat transfer area and performance. Comparison of cyclopentane with respect to other fluids show that adopting a high critical temperature fluid as octane allows to potentially reach higher RTE but it also requires much larger heat transfer area because of the lower fluid density and heat transfer coefficients for average pressure drops. Differently, NOVEC649, having a lower critical temperature, can adopt smaller heat exchangers but it is penalized in cycle thermodynamic leading to a lower RTE.

The proposed methodologies could be a valid method for the selection of a restricted number of working fluid candidates to be further investigated with a detailed techno-economic assessment.

References

[1] B. Cheung, R. Carriveau, and D. S.-K. Ting, “Storing Energy Underwater,” *Mech. Eng.*, vol. 134, no. 12, pp. 38–41, Dec. 2012, doi: 10.1115/1.2012-DEC-3.

[2] M. Astolfi, D. Rizzi, E. Macchi, and C. Spadacini, “A Novel Energy Storage System Based on Carbon Dioxide Unique Thermodynamic Properties,” in *Volume 4: Controls, Diagnostics, and Instrumentation; Cycle Innovations; Cycle Innovations: Energy Storage; Education; Electric Power*, Virtual, Online: American Society of Mechanical Engineers, Jun. 2021, p. V004T07A002. doi: 10.1115/GT2021-59487.

[3] G. Brett and M. Barnett, “The application of liquid air energy storage for large scale long duration solutions to grid balancing,” *EPJ Web Conf.*, vol. 79, p. 03002, 2014, doi: 10.1051/epjconf/20137903002.

[4] R. B. Laughlin, “Pumped thermal grid storage with heat exchange,” *J. Renew. Sustain. Energy*, vol. 9, no. 4, p. 044103, Jul. 2017, doi: 10.1063/1.4994054.

[5] N. R. Smith, J. Just, J. Johnson, and F. Karg-Bulnes, “Performance Characterization of a Small-Scale Pumped Thermal Energy Storage System,” in *Volume 6: Education; Electric Power; Energy Storage; Fans and Blowers*, Boston, Massachusetts, USA: American Society of Mechanical Engineers, Jun. 2023, p. V006T09A012. doi: 10.1115/GT2023-104232.

[6] W. D. Steinmann, “The CHEST (Compressed Heat Energy STorage) concept for facility scale thermo mechanical energy storage,” *Energy*, vol. 69, pp. 543–552, May 2014, doi: 10.1016/j.energy.2014.03.049.

[7] A. H. Hassan, J. M. Corberán, M. Ramirez, F. Trebilcock-Kelly, and J. Payá, “A high-temperature heat pump for compressed heat energy storage applications: Design, modeling, and performance,” *Energy Rep.*, vol. 8, pp. 10833–10848, Nov. 2022, doi: 10.1016/j.egyr.2022.08.201.

[8] D. Alfani, A. Giostri, and M. Astolfi, “Working Fluid Selection and Thermodynamic Optimization of the Novel Renewable-Energy Based RESTORE Seasonal Storage Technology,” in *Volume 6: Education; Electric Power; Energy Storage; Fans and Blowers*, Boston, Massachusetts, USA: American Society of Mechanical Engineers, Jun. 2023, p. V006T09A005. doi: 10.1115/GT2023-103071.

[9] E. Jacquemoud, “Electro-Thermal Energy Storage System (ETES) Based on CO2 Cycles,” in *Encyclopedia of Energy Storage*, Elsevier, 2022, pp. 79–86. doi: 10.1016/B978-0-12-819723-3.00055-X.

[10] J. Miller, “Low-cost, long-duration electrical energy storage using a CO2-based Electro Thermal Energy Storage (ETES) system,”

[11] J. R. Eggers, M. Von Der Heyde, S. H. Thaele, H. Niemeyer, and T. Borowitz, “Design and performance of a long duration electric thermal energy storage demonstration plant at megawatt-scale,” *J. Energy Storage*, vol. 55, p. 105780, Nov. 2022, doi: 10.1016/j.est.2022.105780.

[12] Pintail Power, LLC, Southern Company, NexantECA, and S. Hume, “Liquid Salt Combined-Cycle Pilot Plant Design,” DOE-EPRI-32016-1, 1854364, Feb. 2022. doi: 10.2172/1854364.

[13] Brenmiller Energy, NYPA, United E&C and H. Hack, “Modular, Crushed-Rock Thermal Energy Storage Pilot Design (Final Report),” DOE-EPRI-32017, 1869222, Mar. 2022. doi: 10.2172/1869222.

[14] I. Sarbu and A. Dorca, “Review on heat transfer analysis in thermal energy storage using latent heat storage systems and phase change materials,” *Int. J. Energy Res.*, vol. 43, no. 1, pp. 29–64, Jan. 2019, doi: 10.1002/er.4196.

[15] D. Steger, C. Regensburger, B. Eppinger, S. Will, J. Karl, and E. Schlücker, “Design aspects of a reversible heat pump - Organic rankine cycle pilot plant for energy storage,” *Energy*, vol. 208, p. 118216, Oct. 2020, doi: 10.1016/j.energy.2020.118216.

[16] B. Eppinger, L. Zigan, J. Karl, and S. Will, “Pumped thermal energy storage with heat pump-ORC-systems: Comparison of latent and sensible thermal storages for various fluids,” *Appl. Energy*, vol. 280, p. 115940, Dec. 2020, doi: 10.1016/j.apenergy.2020.115940.

[17] O. Dumont and V. Lemort, “Mapping of performance of pumped thermal energy storage (Carnot battery) using waste heat recovery,” *Energy*, vol. 211, p. 118963, Nov. 2020, doi: 10.1016/j.energy.2020.118963.

[18] H. Jockenhöfer, W.-D. Steinmann, and D. Bauer, “Detailed numerical investigation of a pumped thermal energy storage with low temperature heat integration,” *Energy*, vol. 145, pp. 665–676, Feb. 2018, doi: 10.1016/j.energy.2017.12.087.

[19] G. F. Frate, M. Antonelli, and U. Desideri, “A novel Pumped Thermal Electricity Storage (PTES) system with thermal integration,” *Appl. Therm. Eng.*, vol. 121, pp. 1051–1058, Jul. 2017, doi: 10.1016/j.applthermaleng.2017.04.127.

[20] M. Huber, A. Harvey, E. Lemmon, G. Hardin, I. Bell, and M. McLinden, “NIST Reference Fluid Thermodynamic and Transport Properties Database (REFPROP) Version 10 - SRD 23.” National Institute of Standards and Technology, 2018. doi: 10.18434/T4/1502528.

[21] V. Gnielinski, “New equations for heat and mass transfer in turbulent pipe and channel flow,” 1976. [Online]. Available: https://api.semanticscholar.org/CorpusID:136639967

[22] A. Cavallini *et al.*, “Condensation in Horizontal Smooth Tubes: A New Heat Transfer Model for Heat Exchanger Design,” *Heat Transf. Eng.*, vol. 27, no. 8, pp. 31–38, Sep. 2006, doi: 10.1080/01457630600793970.

[23] M. Mahir, A. El Maakoul, I. Khay, S. Saadeddine, and M. Bakhouya, “An Investigation of Heat Transfer Performance in an Agitated Vessel,” *Processes*, vol. 9, no. 3, p. 468, Mar. 2021, doi: 10.3390/pr9030468.

[24] Z. Liu and R. H. S. Winterton, “A general correlation for saturated and subcooled flow boiling in tubes and annuli, based on a nucleate pool boiling equation,” *Int. J. Heat Mass Transf.*, vol. 34, no. 11, pp. 2759–2766, Nov. 1991, doi: 10.1016/0017-9310(91)90234-6.

[25] A. Žukauskas, “Heat Transfer from Tubes in Crossflow,” in *Advances in Heat Transfer*, vol. 8, Elsevier, 1972, pp. 93–160. doi: 10.1016/S0065-2717(08)70038-8.

[26] M. G. Cooper, “Heat Flow Rates in Saturated Nucleate Pool Boiling-A Wide-Ranging Examination Using Reduced Properties,” in *Advances in Heat Transfer*, vol. 16, Elsevier, 1984, pp. 157–239. doi: 10.1016/S0065-2717(08)70205-3.

[27] T. L. Bergman and F. P. Incropera, Eds., *Fundamentals of heat and mass transfer*, 7th ed. Hoboken, NJ: Wiley, 2011.

[28] J. Blank and K. Deb, “Pymoo: Multi-Objective Optimization in Python,” *IEEE Access*, vol. 8, pp. 89497–89509, 2020, doi: 10.1109/ACCESS.2020.2990567.